Determination of the Sodium Ion Transference Number of the Dion−Jacobson-Type Layered Perovskite $NaCa_2Nb_3O_{10}$ Using ac Impedance and dc Methods

V. Thangadurai and W. Weppner*

Chair for Sensors and Solid State Ionics, Faculty of Engineering, University of Kiel, Kaiserstrasse 2, D-24143 Kiel, Germany

Received July 20, 2001. Revised Manuscript Received December 12, 2001

The electronic conductivity of the Dion−Jacobson-type layered perovskite $NaCa_2Nb_3O_{10}$ was determined by employing ac impedance measurements using ion-blocking electrodes, electron-blocking electrodes, and dc Hebb−Wagner polarization measurements using $NaCoO_2$ as the reversible reference electrode. Oxygen partial-pressure-dependent electrical conductivity studies revealed that the conductivity is nearly independent of the oxygen partial pressure in the range from 0.21 to 10^{-6} atm. Open-circuit voltage measurements of a galvanic cell employing air and 2 ppm of O_2 in argon as electrodes revealed that layered perovskites appear not to be oxide ion conductors. The transference number for Na^+ ions in $NaCa_2Nb_3O_{10}$ at 550 °C is found to be 0.95 at the sodium activity of $NaCoO_2$. The ac measurements using Na-β-alumina with electron-blocking electrodes and Pt-nonblocking electrodes produced similar impedance data at 550 °C suggesting a high ionic nature, which is consistent with the polarization study. However, the ionic and electronic conductivities varied depending on the experimental conditions, such as temperature and partial pressures.

1. Introduction

Lamellar titanates/niobates form an important class of materials in view of their unique properties. In general, two types of lamellar oxides are known: (i) Ruddlesden−Popper[1] (R−P) phases with the general formula $A_2[A'_{n-1}B_nO_{3n+1}]$ and (ii) Dion−Jacobson[2] (D−J) phases with the general formula $A[A'_{n-1}B_nO_{3n+1}]$, where A is a mono- or divalent ion, A′ is a di- or trivalent ion, and B is a tetra- or pentavalent metal ion. These are also called layered perovskites. Historically, R−P phases have been known since 1957 to be formed in the Sr−Ti−O system, whereas the D−J phases were first synthesized more recently in 1981.[2] The number n determines the number of BO_6 octahedra connected by their corners along the c axis. The idealized structure of the $n = 3$ member of the D−J phase is shown in Figure 1. Typical examples of members of both phases, which can be found in refs 1−5, exhibit technologically interesting chemical and physical features. For example, both phases show appreciable electrical conductivity,[5d,6] dielectricity,[7] ion-exchange reactions,[2,3] intercalation and deintercalation, and giant magnetoresistivity (GMR),[8] and both can be used as photocatalysts[9] for water decomposition.

A substantial amount of work has been performed on both R−P and D−J phases to understand the structure−composition−property relations. For example, the reactivities of both phases with respect to the ion-exchange and acidity of solid acids were investigated.[2,3] Of the two types of phases, the D−J phases exhibit several superior properties compared to R−P phases such as fast ion exchange and high electrical conductiv-

* Author to whom correspondence should be addressed. E-mail: ww@tf.uni-kiel.de. Fax: 0049 431 880 6203.

(1) Ruddlesden, S. N.; Popper, P. *Acta Crystallogr.* **1957**, *10*, 538; **1958**, *11*, 54.

(2) Dion, M.; Ganne, M.; Tournoux, M. *Mater. Res. Bull.* **1981**, *16*, 1429. (b) Jacobson, A. J.; Johnson, J. W.; Lewandowski, J. T. *Inorg. Chem.* **1985**, *24*, 3727. (c) Jacobson, A. J.; Lewandowski, J. T.; Johnson, J. W. *J. Less Common. Met.* **1986**, *116*, 137. (d) Gopalakrishnan, J.; Bhat, V.; Raveau, B. *Mater. Res. Bull.* **1987**, *22*, 413.

(3) Blasse, G. *J. Inorg. Nucl. Chem.* **1968**, *30*, 656. (b) Dion, M.; Ganne, M.; Tournoux, M. *Rev. Chim. Miner.* **1986**, *23*, 61. (c) Gopalakrishnan, J.; Bhat, V. *Inorg. Chem.* **1987**, *26*, 4299. (d) Uma, S.; Raju, A. R.; Gopalakrishnan, J. *J. Mater. Chem.* **1993**, *3*, 709. (e) Richard, M.; Brohan, L.; Tournoux, M. *J. Solid State Chem.* **1994**, *112*, 354.

(4) Toda, K.; Teranishi, T.; Ye, Z. G.; Sato, M.; Hinatsu, Y. *Mater. Res. Bull.* **1999**, *34*, 971. (b) Hyeon, K. A.; Byeon, S. H. *Chem. Mater.* **1999**, *11*, 352. (c) Kodenkandath, T. A.; Lalena, J. N.; Zhou, W. L.; Carpenter, E. E.; Sangregorio, C.; Falster, A. U.; Simmons, W. B.; O'Connor, C. J.; Wiley, J. B. *J. Am. Chem. Soc.* **1999**, *121*, 10743. (d) Gopalakrishnan, J.; Sivakumar, T.; Thangadurai, V.; Subbanna, G. N. *Inorg. Chem.* **1999**, *38*, 2802.

(5) Schaak, R.; Mallouk, T. E. *J. Solid State Chem.* **2000**, *155*, 46. (b) Byeon, S. H.; Nam, H. J. *Chem. Mater.* **2000**, *12*, 1771. (c) Lalena, J. N.; Falster, A. U.; Simmons, W. B.; Carpenter, E. E.; Wiggins, J.; Hariharan, S.; Wiley, J. B. *Chem. Mater.* **2000**, *12*, 2418. (d) Thangadurai, V.; Beurmann, P. S.; Weppner, W. *J. Solid State Chem.* **2001**, *158*, 279.

(6) Sato, M.; Abo, J.; Ohta, M. *J. Alloys Compd.* **1993**, *192*, 81. (b) Sato, M.; Watanabe, J.; Uematsu, K. *J. Solid State Chem.* **1993**, *107*, 460. (c) Thangadurai, V.; Weppner, W. *J. Mater. Chem.* **2001**, *11*, 636. (d) Choy, J. H.; Kim, J. Y.; Kim, S. J.; Sohn, J. S.; Han, O. H. *Chem. Mater.* **2001**, *13*, 906.

(7) Fang, M.; Kim, C. H.; Mallouk, T. E. *Chem. Mater.* **1999**, *11*, 1519.

(8) Moritomo, Y.; Asamitsu, A.; Kuwahara, H.; Tokura, Y. *Nature* **1996**, *380*, 141. (b) Battle, P. D.; Blundell, S. J.; Green, M. A.; Hayes, W.; Honold, M.; Klehe, A. K.; Laskey, N. S.; Millburn, J. E.; Murphy, L.; Rosseinsky, M. J.; Samarin, N. A.; Singleton, J.; Sluchanko, N. E.; Sullivan, S. P.; Vente, J. F. *J. Phys.: Condens. Matter* **1996**, *8*, L427. (c) Seshadri, R.; Martin, C.; Hervieu, M.; Raveau, B.; Rao, C. N. R. *Chem. Mater.* **1997**, *9*, 270.

(9) Ebina, Y.; Tanaka, A.; Kondo, J. N.; Domen, K. *Chem. Mater.* **1996**, *8*, 2534. (b) Takata, T.; Furumi, Y.; Shinohara, K.; Tanaka, A.; Hara, M.; Kondo, J. N.; Domen, K. *Chem. Mater.* **1997**, *9*, 1063.

10.1021/cm011189w CCC: $22.00
Published on Web 02/21/2002

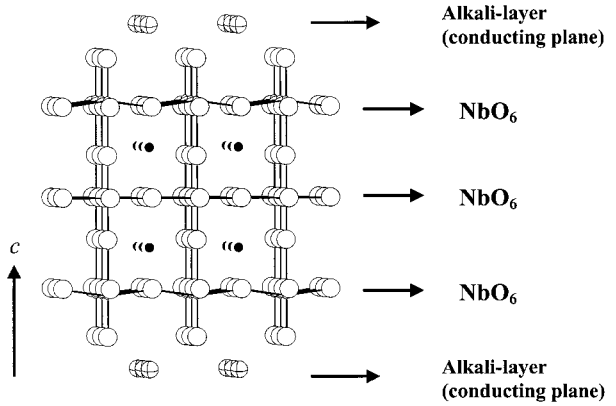

Figure 1. Idealized structure of the $n = 3$ D−J-type layered perovskite $NaCa_2Nb_3O_{10}$.

ity.[2,6] However, thus far, the electrical conductivities of both types of phases have not been investigated in detail with regard to the electronic and ionic contributions.[1−7] The observed electrical conductivity is assumed to be mainly ionic due to the migration of interlayer alkali ions in layered perovskites.[6] Furthermore, on the basis of the fast ion exchange and the 2D layered structure, the D−J and R−P phases are considered to be electronically insulating.

The main objective of the present work is to investigate the partial ionic and electronic (both hole and excess electron) contributions to the total conductivity of a typical D−J-type layered perovskite. For a detailed study, we have considered the first known D−J phase,[2a] i.e., the $n = 3$ member $NaCa_2Nb_3O_{10}$ of the series $ACa_2Nb_3O_{10}$ (A = Li, Na, K, Rb, Cs). The applied method is based on an analysis of steady-state polarization curves using an ion-blocking electrode in combination with a reversible electrode according to the theory of Hebb and Wagner (HW),[10] which has been found to provide more reliable results for predominant ionic conductors.

2. Theoretical Considerations

2.1. Determination of the Transference Numbers. A common method of determining the transference number (t_{Na}) of Na^+ ions in $NaCa_2Nb_3O_{10}$ is the application of a galvanic cell under zero current with the sample sandwiched between two materials of different, but fixed, sodium activities.[11] The EMF (E) of the cell can be derived from the overall charge compensation of the fluxes of all charge carriers in the case of zero total electrical current i[12]

$$E = -\int_{'}^{''} \Sigma \frac{t_k}{z_k F} \, d\mu_k \qquad (1)$$

where z_k, F, and μ_k are the charge number of species k, Faraday's constant, and the chemical potential of the neutral species k^x, respectively. The summation runs over all species k except the electronic charge carrier e.

In practice, it is common to compare the measured EMF (E_{exp}) with the theoretical one (E_{Nernst}) expected for a pure ionic conductor of ion k according to the Nernst equation. This results in an average transference number, which depends on the chemical potentials of the neutral component k^x at both electrode sides

$$\bar{t}_k(\mu'_k, \mu''_k) = \frac{E_{exp}}{E_{Nernst}} = \frac{\int_{'}^{''} t_k \, d\mu_k{}^x}{\mu''_k{}^x - \mu'_k{}^x} \qquad (2)$$

Experimentally, fixing the sodium activity by using elemental sodium is difficult. Furthermore, Nb^V in $NaCa_2Nb_3O_{10}$ in contact with elemental sodium will be easily reduced at elevated temperature. Therefore, we adopted the dc polarization technique, the so-called Hebb−Wagner (HW) method,[10] using $NaCoO_2$ as the reference electrode and combined the method with impedance measurements.

The HW polarization method has been developed to determine the minority charge carrier conductivity of predominant ionic conductors. Previously, this technique has been employed for the determination of the hole and excess electronic conductivities of silver ion conductors[13] and zirconia-[14] and ceria-[15] based oxide ion electrolytes.

The total electrical conductivity (σ_t) of $NaCa_2Nb_3O_{10}$ is the sum of the contributions of all ions, excess electrons, and holes. Because both Ca^{2+} and Nb^{5+} ions occupy the perovskite blocks (Figure 1) with 12- and 6-oxygen coordinations, it is assumed that their mobilities can be neglected. Accordingly

$$\sigma_t = \sigma_{Na^+} + \sigma_{O^{2-}} + \sigma_{e^-} + \sigma_h. \qquad (3)$$

The contributions of excess electrons and holes can be obtained from polarization measurements using sodium and oxide ion-blocking electrodes. Hence, the partial conductivity of sodium ions can be determined from the total, oxide ion, excess electronic, and hole conductivities.

2.2. Determination of Partial Electronic (Electrons and Holes) Conductivity. For the measurement of the partial electronic (both excess and defect electronic) conductivity by the HW method, the following cell was employed (Figure 2a)

$$(-)\ Pt,\ NaCoO_2\ |NaCa_2Nb_3O_{10}|\ Pt\ (+)$$
(argon atmosphere) (I)

The exchange of oxygen at the electrodes was prevented by the use of dense Pt electrodes and a sealed left-hand reference side with a high-temperature sealant (zirconia-based powder). The pure Ar gas environment further restricted interactions with the surrounding atmosphere. Under a dc potential of less than the voltage that might decompose the sample, all charge carriers

(10) Hebb, M. H. *J. Chem. Phys.* **1952**, *20*, 185. (b) Wagner, C. In *Proceedings of the 7th Meeting of the International Committee on Thermodynamic and Kinetic Electrochemistry (CITCE), Lindau, Germany, 1955*; Butterworth Publications: London, 1957; p 361.

(11) Weppner, W.; Huggins, R. A. *Annu. Rev. Mater. Sci.* **1978**, *8*, 269. (b) Tuller, H.L. In *Nonstoichiometric Oxides*; Sorensen, O. T., Ed.; Academic Press: New York, 1981.

(12) Rickert, H. *Electrochemistry of Solids: An Introduction*; Springer-Verlag: Berlin, 1982. (b) Wagner, C. In *Advances in Electrochemical Engineering*; Delahay, P.; Tobias, C., Eds.; Interscience: New York, 1966. (c) Schmalzried, H. *Z. Phys. Chem.* **1963**, *38*, 87. (d) Thangadurai, V.; Weppner, W., to be published.

(13) Weppner, W.; Liu, J. *Z. Naturforsch.* **1991**, *46*, 409.

(14) Weppner, W. *Electrochim. Acta* **1977**, *22*, 721. (b) Kopp, A.; Näfe, H.; Weppner, W. *Solid State Ionics* **1992**, *53−56*, 853.

(15) Lübke, S.; Wiemhöfer, H. D. *Solid State Ionics* **1999**, *117*, 229.

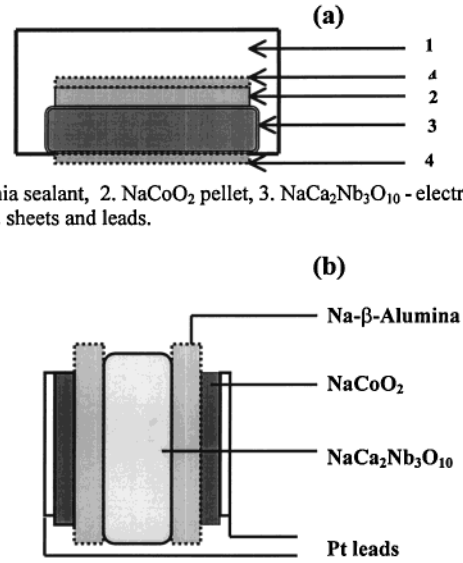

Figure 2. Schematic diagram of (a) Hebb−Wagner (HW) polarization cell (sample thickness = 1.2 or 2 mm and diameter = 9.5 mm) and (b) electron-blocking cell (sample thickness = 1.4 mm and diameter = 9.5 mm), both of which were used for dc and ac measurements.

migrate initially, but only electrons and holes move under steady-state conditions.[12] The current is due to the applied voltage and the diffusion of electronic charge carriers in the concentration gradient that is established. It is assumed that the mobilities of both holes and electrons are independent of the concentrations and that the contact resistances for the electronic charge carriers at the electrode/electrolyte interfaces are negligible.

Under the passage of a dc current through the cell with positive polarity at the right-hand side (Pt), only electronic charge carriers can flow through the cell as Na^+ ions cannot be replaced at the Pt side. The steady-state current density i of electrons and holes is determined using the equation[10]

$$i = \frac{kT}{qL}\left[\sigma_e\left(\exp\left(\frac{-Uq}{kT}\right) - 1\right) + \sigma_h\left(1 - \exp\left(\frac{Uq}{kT}\right)\right)\right] \quad (4)$$

where k, T, q, L, and U are the Boltzmann constant, the absolute temperature, the elementary charge, the length of the sample (distance between the electrodes), and the applied voltage, respectively. A simple two-band model[15] with the Fermi level within the gap and far from the electronic energies is assumed. Accordingly, the applied voltage results in a difference in the electronic charge carrier concentration rather than in the electrostatic potential. The first term in the square brackets approaches a plateau caused by the excess electron conductance, whereas the second term represents an exponential increase caused by the hole conductance. The conductivities of excess electrons and holes at the composition fixed by the equilibrium with the reversible reference electrode are determined from the height of the plateau and the intersection of the exponential increase with the current axis in a current−voltage plot.

The dependences of the electron and hole conductivities on the sodium activity are derived from the exchange reaction of sodium with the lattice of $NaCa_2Nb_3O_{10}$, which can be written in terms of Kroeger−Vink elements as

$$Na(a_{Na}) + V_i = Na_i^{\bullet} + e' \quad (5)$$

where V_i, $Na_i^{\bullet}$, and e' represent a vacancy at an interstitial position, a Na ion at an (interstitial) interlayer position,[2,16] and an excess electron, respectively. The mass action law for this reaction reads

$$a_{Na}/a_{Na_i^{\bullet}}a_{e'} = \text{constant} \quad (6)$$

where a represents the activity. For an ionic conductor, it is assumed that the concentration of mobile ionic defects is large and can be considered constant, in agreement with the validity of the HW eq 4.[10]

$$c_{Na_i^{\bullet}} = \text{constant} \quad (7)$$

Assuming that the activity coefficients of the electrons and sodium ions are approximately constant, the following relation between the sodium activity and concentration of electrons can be obtained

$$\mathrm{d}\log c_{e'}/\mathrm{d}\log a_{Na} = 1 \quad (8)$$

By considering the fact that the partial conductivity is proportional to the concentration of the corresponding species, one can show that

$$\mathrm{d}\log \sigma_e = \mathrm{d}\log a_{Na} \quad (9)$$

Because of the equilibrium between electrons e^- and holes $h^{\bullet}$ ($c_{e'}c_{h^{\bullet}}$ = constant), i.e.

$$\mathrm{d}\log c_{e'} = -\mathrm{d}\log c_{h^{\bullet}} \quad (10)$$

the inverse slope holds for the conduction of holes.

$$\mathrm{d}\log \sigma_{h^{\bullet}} = -\mathrm{d}\log a_{Na} \quad (11)$$

3. Experimental Aspects

$NaCa_2Nb_3O_{10}$ was prepared from $KCa_2Nb_3O_{10}$ by ion-exchange reaction using molten $NaNO_3$. The ion-exchange reaction was carried out for 10 days with intermittent washing after 5 days. $KCa_2Nb_3O_{10}$ was prepared by solid-state reaction between metal carbonates and oxides at 1250 °C for 24 h.[2] An excess of 20 wt % alkali carbonate was added for compensation of the alkali oxide loss as a result of volatilization. Powder X-ray diffraction (XRD) using a Seifert 3000 (Cu K_α) powder X-ray diffractometer at room temperature was employed to detect the phase formations. Thermogravimetric analysis (TGA) was performed in air using a Netzsch thermal analyzer (model STA 409) for the identification of the composition/decomposition processes. Energy-dispersive X-ray (EDX) analysis measurements were carried out to verify the completion of the ion-exchange reaction, and scanning electron microscopy (SEM) was employed for surface morphology studies of the layered perovskites before and after the electrical measurements by employing a Philips SEM XL 30 electron microscope.

Powdered $NaCa_2Nb_3O_{10}$ was pressed into a pellet (diameter, 9.5 mm; thickness, ~1.5 mm) and sintered at 1000 °C for 24 h in air. The pellet was covered with the same powder during sintering to minimize losses of alkali metal and oxides due to volatilization. The flat pellet surface was coated with Pt paste,

(16) Armstrong, A. R.; Anderson, P. A. *Inorg. Chem.* **1994**, *33*, 4366. (b) Bohnke, C.; Bohnke, O.; Fourquet, J. L. *J. Electrochem. Soc.* **1997**, *144*, 1151. (c) Fukuoka, H.; Isami, T.; Yamanaka, S. *J. Solid State Chem.* **2000**, *151*, 40.

which was cured at 850 °C for 1 h to remove the organic binders and obtain good adhesion. ac impedance measurements were made using a HP 4192 A impedance and gain phase analyzer in the frequency range from 5 Hz to 13 MHz between 400 and 800 °C. The electrical conductivity data were measured under different oxygen partial pressures in the range from 0.21 to 10^{-6} atm at 800 °C. The oxygen partial pressures were established by mixing Ar with 1000 ppm of oxygen in Ar using Tylan mass flow controllers. The exact oxygen partial pressures of the gas mixtures were determined by using potentiometric YSZ oxygen sensors operating at 700 °C.

Hebb−Wagner[10] (HW) polarization measurements were performed at 550 °C using the arrangement shown in Figure 2a with $NaCoO_2$ as the reference material. Voltages between 0 and 2 V were applied. The current was measured as a function of time by using a potentiostat (PG 2.0, Ionic Systems). The excess electron and hole conductivity values were determined by fitting the experimental data to eq 4. The sodium ion conductivity of $NaCa_2Nb_3O_{10}$ was determined by both ac measurements (500−800 °C) and dc experiments using commercially available Na-β-alumina as the electron-blocking electrodes (550 °C), as shown in Figure 2b. Voltages between 0 and 1 V were applied in both increasing and decreasing voltage directions.

4. Results and Discussion

4.1. Phase Analysis and Total Conductivity. Both powder XRD and EDX data reveal complete K^+/Na^+ exchange reactions. The EDX data for the ion-exchanged product show that the samples are homogeneous and that the ratio of Na to Ca to Nb in several crystallites is 1:2:3, which corresponds with the expected value for the nominal composition and confirms the completeness of the ion-exchange reaction. The TGA data show that the ion-exchanged product is hydrated and loses one water molecule per formula unit at about 400 °C. The results are consistent with the literature data.[2] Accordingly, we increased the sample temperature to 750 °C and maintained this temperature for about 12 h before performing the impedance measurements. In this way, possible contributions from proton conduction to the total conductivity due to water can be expected to be excluded.

Figure 3a shows a typical impedance plot obtained in air at 550 °C. We observed one arc and a tail at the low-frequency side, which is a behavior typical of ion blocking at the interfaces.[17] Upon heating, the tail was more pronounced. The high-frequency arc could be resolved into two semicircles, corresponding to bulk and grain-boundary contributions. The electrical conductivity data were taken from the minimum of the corresponding admittance plot (Figure 3b). Because the intercept combines both bulk and grain-boundary contributions to the total resistance, the value obtained here was considered to be the total conductivity. Arrhenius diagrams for the total electrical conductivity σ and σT are shown in Figure 4. The conductivity data obtained from the cooling and heating parts follow the same line. The activation energy for the electrical conduction is 0.72 eV, which is considerably higher than the values obtained for the cases of Na-β-alumina (0.16 eV)[18] and $Na_3Zr_2Si_2PO_{12}$ (0.15 eV).[19] However, the obtained value is comparable to those of Li_4SiO_4, Sr-

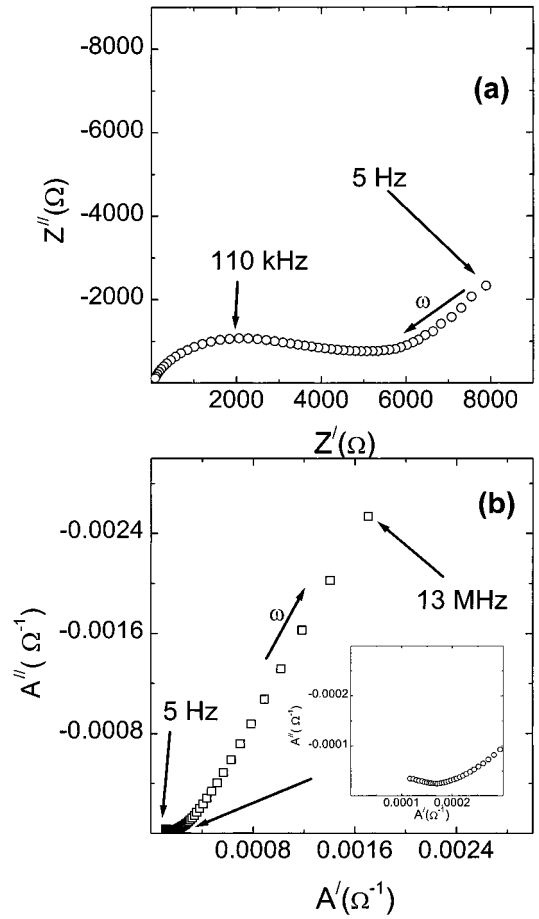

Figure 3. Typical impedance plot (top) obtained in air at 550 °C using ion-blocking Pt electrodes. The bottom figure shows the corresponding admittance data. The inset shows the data on an expanded scale.

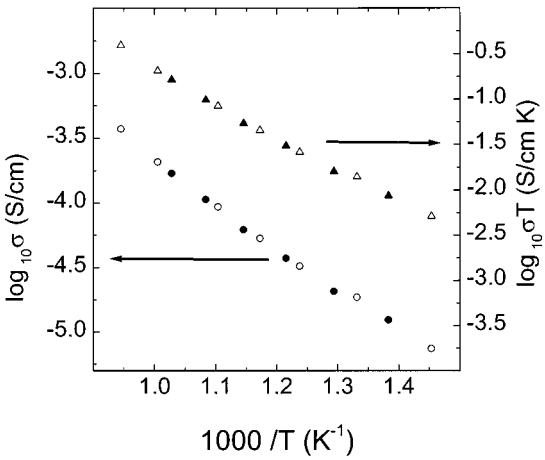

Figure 4. Arrhenius plots for the total electrical conductivity (σ and σT) of $NaCa_2Nb_3O_{10}$ in air. The activation energy for the electrical conduction is 0.72 eV. The open and closed symbols represent data obtained during cooling and heating runs, respectively.

CeO_3:Y, and YSZ.[19] The ionic conductivities of the n = 2 and 3 members of the D−J phases are of the same order of magnitude (Table 1).

(17) Watanabe, H.; Kuwano, J. *J. Power Sources* **1997**, *68*, 421. (b) Losilla, E. R.; Aranda, M. A. G.; Bruque, S.; Sanz, J.; Paris, M. A.; Campo, J.; West, A. R. *Chem. Mater.* **2000**, *12*, 2134.

(18) Colomban, Ph., Ed. *Proton Conductors Solids, Membranes and Gels- Materials and Devices*; Cambridge University Press: New York, 1992.

(19) Greenblatt, M. In *Encyclopaedia of Inorganic Chemistry*; King, R. B., Ed.; John Wiley: Chichester, U.K., 1994; p 1584.

Table 1. Comparison of Electrical Conductivity Data for $NaCa_2Nb_3O_{10}$ with That for Other 2D and 3D Cation and Oxide Ion Conductors[2a,6a,18,19]

compound	dimensionality	σ (S/cm), temp (°C)	E_a (eV)
$NaCa_2Nb_3O_{10}$	2D	1.0×10^{-5}, 440	0.72
$NaLaNb_2O_7$	2D	3.5×10^{-5},440	0.30
$KLaNb_2O_7$	2D	3.5×10^{-6},440	0.25
$KCa_2Nb_3O_{10}$	2D	4.4×10^{-6}, 440	0.86
Na-β-alumina	2D	3.0×10^{-2}, RT[a]	0.16
Li_3N	2D	5.0×10^{-3}, RT[a]	0.30
Li-β-alumina	2D	1.3×10^{-3}, 200	0.19
H_3O-β-alumina	2D	$\sim 10^{-10}$, RT[a]	0.80
$Na_3Zr_2Si_2PO_{12}$ (NASICON)	3D	10^{-1}, 300	0.15
NASICON glassy	3D	10^{-4}, 600	0.65
Li_2SO_4	3D	1.04, 600	0.40
Li_4SiO_4	3D	2.2×10^{-3}, 400	0.74
$Li_{14}Zn(GeO_4)_4$ (LISICON)	3D	1.7×10^{-4}, 200	0.50
$SrCeO_3$:Y	3D	10^{-6}, RT[a]	0.63
ZrO_2.9% Y_2O_3 (YSZ)	3D	0.12, 1000	0.80

[a] RT = room temperature.

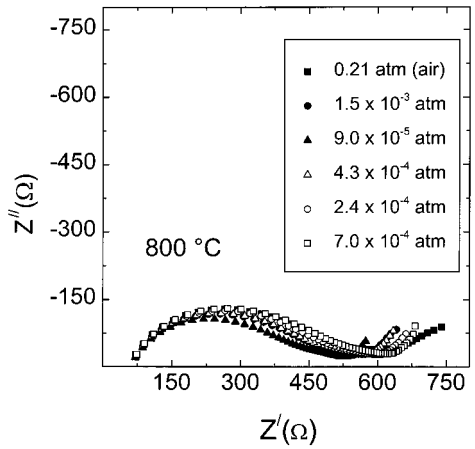

Figure 5. Impedance at 800 °C as a function of the oxygen partial pressure.

4.2. Determination of Oxide Ion Contribution. Figure 5 shows impedance plots for different oxygen partial pressures at 800 °C. Very little change occurs in the resistance for pressures ranging from 0.21 to about 10^{-6} atm, indicating that oxide ions and electrons might be mobile in $NaCa_2Nb_3O_{10}$. However, the resistance changes by only about 0.1 order for nearly 4 orders of change in the oxygen partial pressure. Accordingly, the contribution to the total conductivity is very small.

To obtain additional direct information on the contribution of the oxide ion conduction, we measured the open-circuit voltages for a galvanic cell employing $NaCa_2Nb_3O_{10}$ as the separator between air or oxygen at one side and argon gas with an oxygen partial pressures of ~2 ppm at the other side at various temperatures (Figure 6). No Nernstian EMF for the galvanic cell was seen; the observed values were much lower. In the presence of water vapor, the same results were found, suggesting that oxide ion (O^{2-}) or proton (H^+, H_3O^+, OH^-) conduction does not play a role in the investigated sample. Accordingly, we assumed that the measured conductivity in air was due to the contributions of alkali ions and electrons.

4.3. Hebb−Wagner (HW) Polarization Study. Typical time responses of the current in HW measurements (1.2- or 2-mm thickness of the electrolyte) at 650 and 800 mV are shown in Figure 7. We see a very fast

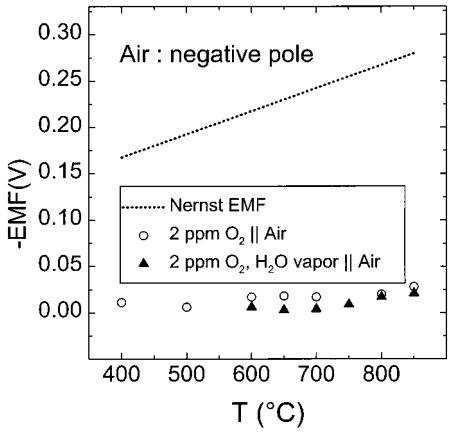

Figure 6. Open-circuit voltages of a galvanic cell using $NaCa_2Nb_3O_{10}$ as the electrolyte for air or oxygen at one side and 2 ppm O_2 in Ar at the other side. The calculated Nernst EMF for the cell is also shown.

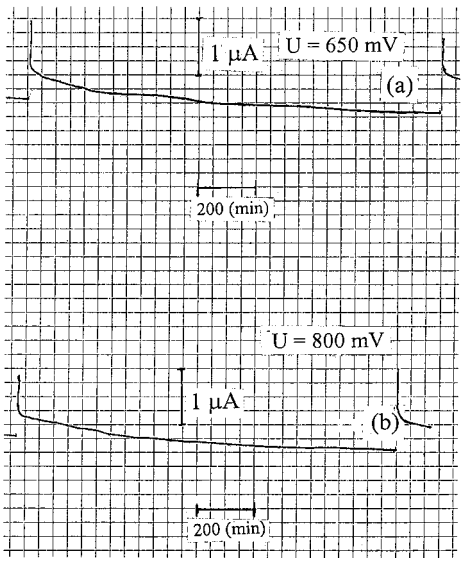

Figure 7. Typical time dependence of the current after application of voltages of (a) 650 and (b) 800 mV at 550 °C in Hebb−Wagner (HW) experiments.

response at the beginning, followed by a much slower change in current at a given voltage. Figure 8 presents the steady-state current as a function of the applied voltage. We see a plateau current in the range 0.5−1.5 V and a subsequent slow increase of the current. Employing the HW theory, the excess electron minority charge carrier conductivity (σ_e) was measured to be 2.05×10^{-6} S/cm at 550 °C, which is an order of magnitude lower than the total, i.e., mainly ionic, conductivity. The dotted line in Figure 8 shows the current calculated using eq 4 with an electronic conductivity of 2.05×10^{-6} S/cm at 550 °C. We see that the calculated line fits the experimental data points well up to 1.5 V; the increase in current above 1.5 V might be due to hole conduction or decomposition of the sample. The sodium ion transference number according to the equation $t_{Na} = [\sigma_t - (\sigma_e + \sigma_h)]/\sigma_t$ was found to be 0.95 ($\sigma_t = 3.75 \times 10^{-5}$ S/cm, $\sigma_e = 2.05 \times 10^{-6}$ S/cm, σ_h is considered to be a very small quantity and is therefore neglected) at equilibrium of the sample with $NaCoO_2$.[20]

(20) Schettler, H. Ph.D Thesis, Faculty of Chemitry and Pharmacy, University of Tübingen, Tübingen, Germany, 1994.

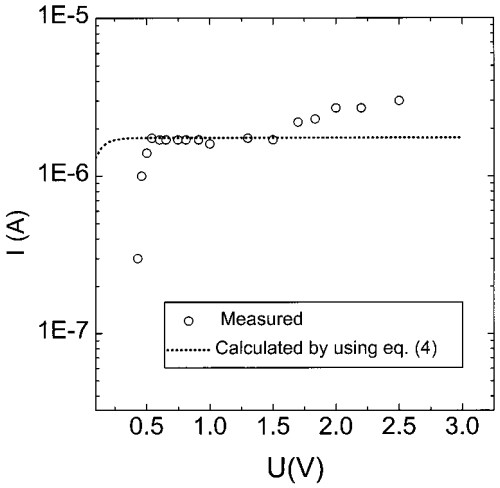

Figure 8. Hebb−Wagner (HW) curve: steady-state current as a function of the applied voltage at 550 °C. The increase in current above 1.5 V is considered to be due to decomposition. The broken line passing through the plateau data points below 1.5 V was obtained by fitting the data to eq 4. The electronic conductivity used in this calculation was 2.05×10^{-6} S/cm.

Table 2. Comparison of Diffusion Coefficients of Electrons in $NaCa_2Nb_3O_{10}$ with Those of Other Ionic Conductors

compound	diffusion coefficient (cm^2/s), temp (°C)	ref
$NaCa_2Nb_3O_{10}$	6.7×10^{-7}, 550	present study (polarization)
$NaCa_2Nb_3O_{10}$	6.5×10^{-7}, 550	present study (conductivity)
ZrO_2 10 mol % Y_2O_3	8.9×10^{-4}, 700	14a
ZrO_2 10 mol % Y_2O_3	2.0×10^{-3}, 900	14a
$La_{0.9}Sr_{0.1}Ga_{0.8}Mg_{0.2}O_{2.85}$	1.1×10^{-7}, 600	21a
$La_{0.992}Ca_{0.008}AlO_3$	1.2×10^{-6}, 800	21b
$LaCoO_3$	3.1×10^{-6}, 800	21b
$RbSr_2Nb_3O_{10}$	6.8×10^{-8}, 620	5d (conductivity)

This value can vary if other reference materials are used.[11,12]

The chemical diffusion coefficient ($\tilde{D}$), which was assumed to be controlled by the diffusion coefficient of the electrons (D_e), was calculated from the time required to establish the new steady-state current after a voltage step was applied by using the formula $D_e = L^2/\tau$, where L is the thickness of the electrolyte and τ is the equilibration time. The diffusion coefficient was obtained by assuming an equilibration time of 1000 min, and the data were compared with values obtained for other ionic conductors (Table 2). It is interesting to note that the value obtained is comparable to those of YSZ[14a] and LSGM[21a] oxide ion electrolytes.

We found that the impedance of the system (polarization cell in Figure 2a) increased by a factor of about 3 after the polarization measurements (Figure 9). To understand this behavior further, we performed EDX and SEM analyses. These data showed that the surface in contact with $NaCoO_2$ was not affected. We did not see any reaction products at the white interface surfaces. However, a very large increase in particle size was observed after the polarization measurements (Figure 10b). Sintering during the long annealing time used for the polarization measurements might have caused this increase in particle size. In turn, it is expected that the grain-boundary resistance would decrease. It is therefore more likely that the increase in impedance was due to the voltage applied to the sample. Generally, the application of voltages to any material results in a change in its original composition.

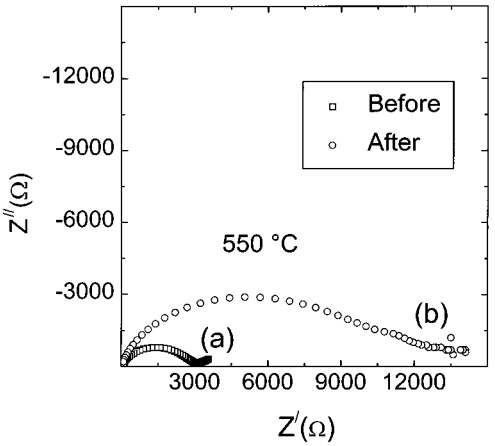

Figure 9. Impedance data (a) before and (b) after Hebb−Wagner (HW) polarization measurements.

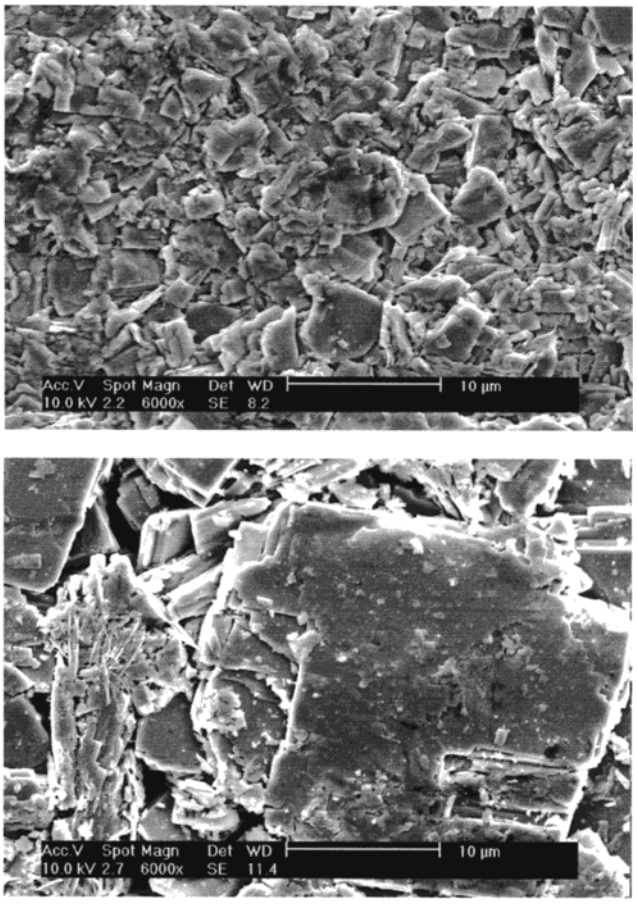

Figure 10. SEM photograph of $NaCa_2Nb_3O_{10}$ at the reference side before (top) and after (bottom) the polarization measurements. The data show the absence of chemical reactions between $NaCa_2Nb_3O_{10}$ and $NaCoO_2$. The increase in particle size (bottom) after polarization measurements is clearly seen.

4.4. Electron-Blocking ac Method. We also determined the ionic conductivity by ac impedance measurements using electron-blocking Na-β-alumina electrodes

(21) Schmidt, S.; Berckemeyer, F.; Weppner, W. *Ionics* **2000**, *6*, 139. (b) Mizusaki, J. *Solid State Ionics* **1992**, *52*, 79.

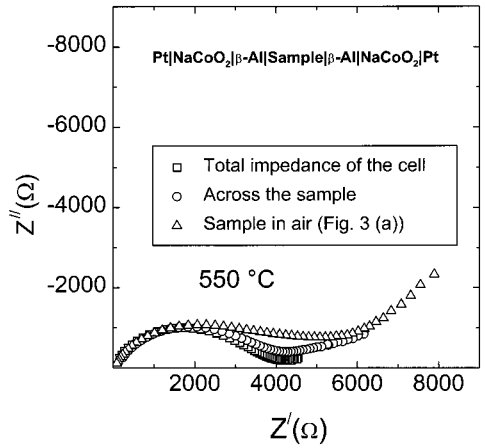

Figure 11. Typical impedance plots obtained for $NaCa_2Nb_3O_{10}$ at 550 °C using electron-blocking Na-β-alumina electrodes compared to that obtained using nonblocking Pt electrodes at the same temperature (sample thickness = 1.4 mm and diameter = 9.5 mm).

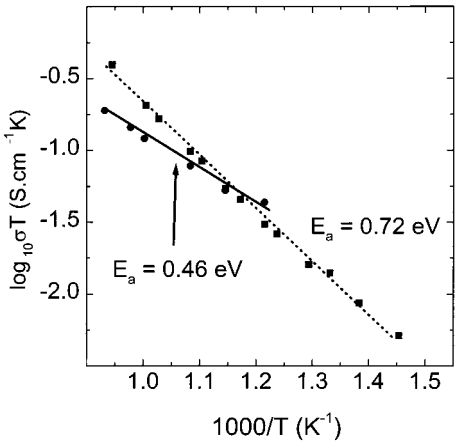

Figure 12. Comparison of Arrhenius plot for the electrical conductivity of $NaCa_2Nb_3O_{10}$ obtained using non-electron-blocking Pt electrodes (squares) and electron-blocking Na-β-alumina electrodes (circles) by ac impedance.

(Figure 2b). Typical impedance plots obtained at 550 °C are shown in Figure 11. Very interestingly, we see nearly the same bulk contribution (high-frequency part) to the total conductivity for both electron-blocking Na-β-alumina and nonblocking Pt electrodes. The impedance results reveal that apparently no contribution arises from the contact resistance in the galvanic cell. If a contact resistance existed in addition to the sample resistance, we would expect to observe a much higher impedance. Figure 12 compares Arrhenius plots for electrical conductivity obtained from both the electron-blocking and nonblocking measurements. The conductivity in the case of the Na-β-alumina electron-blocking electrodes appears to be slightly lower, especially at high temperatures. This effect might be due to a slow increase in interfacial resistance between the β-alumina and the sample.

4.5. Non-Electron-Blocking dc Method. The dc measurements with fixed sample sodium activity, which was applied by short-circuiting both Na-β-alumina (Figure 2b) auxiliary electrolytes, show an exponential increase of the current in the voltage range from 0.4 to 1 V (Figure 13). Only electronic charge carriers are transferred in the steady state in this type of experiment. The conductivity value obtained from the slope is 2.0×10^{-6} S/cm, which is close to the electronic conductivity value (2.05×10^{-6} S/cm) obtained from the HW polarization measurements.

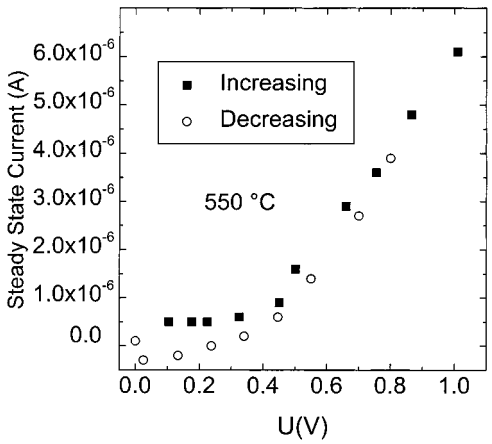

Figure 13. Steady-state dc electrical current measurement at 550 °C with fixed sodium activity on both sides of the electrolyte sample. The thickness of the sample is 1.4 mm, and the diameter is 9.5 mm. An exponential increase in the electrical current above 0.4 V is clearly seen. The steady-state current is due to electronic conduction only.

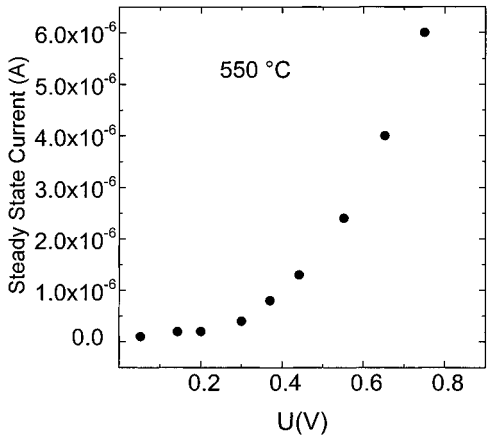

Figure 14. Steady-state dc electrical current measurement at 550 °C with fixed sodium activity on the left-hand side (which is at negative polarity compared to the right-hand side). The thickness of the sample is 1.4 mm, and the diameter is 9.5 mm. An exponential increase in the electrical current above 0.4 V is clearly seen. Only an ionic current occurs at steady state.

4.6. Electron-Blocking dc Method. Only one of the Na-β-alumina auxiliary electrolytes (left-hand) was short-circuited in the another experiment, and the results are shown in Figure 14. In this case, the sodium activity was controlled at the left-hand side of the sample, while the other Na-β-alumina electrolyte blocked any electronic current. The purely ionic current (in the steady state) was controlled by the motion of sodium ions in the electrochemical potential gradient. If the chemical potential of sodium ions could be considered to be approximately constant, the current would be determined by the electrical field. A linear relationship, as expected according to Ohm's law, was observed at higher voltages. The slope indicates a higher conductivity than in the case of merely the transport of electrons (Figure 14), which is, however, smaller than the expected value according to the ac impedance measure-

Table 3. Comparison of Partial Electronic Conductivity and Activation Energy Data for $NaCa_2Nb_3O_{10}$ with Values for Other Well-Known Ionic Conductors in the Literature

compound	σ_e (S/cm), temp (°C)	$E_{a,e}$ (eV)	σ_h (S/cm), temp (°C)	$E_{a,h}$ (eV)	ref
$NaCa_2Nb_3O_{10}$	1.3×10^{-6}, 600[a]	1.68	–	–	present work
Na-β-alumina	8.47×10^{-7}, 350	–	2.5×10^{-11}, 350	–	13
Ca-β-alumina	2.0×10^{-6}, 635	1.88	$\sim 10^{-16}$, 635	1.83	13
Cu-β-alumina	1.3×10^{-7}, 727	3.35	1.6×10^{-8}, 727	3.17	13
Ag-β-alumina	1.7×10^{-7}, 550	1.32	$<10^{-11}$, 500	–	13
$Ce_{0.8}Gd_{0.2}O_{1.9}$	1.4×10^{-6},600	2.59	4.7×10^{-6}, 600	1.16	15
$Ce_{0.8}Gd_{0.17}Pr_{0.03}O_{1.9}$	3.2×10^{-6},600	2.38	1.6×10^{-4}, 600	0.70	15
ZrO_2 10 mol % Y_2O_3	7.5×10^{-7}, 900	4.4	6.5×10^{-6}, 900	1.7	12a
$La_{0.9}Sr_{0.1}Ga_{0.8}Mg_{0.2}O_{2.85}$	$\sim 10^{-16}$, 600	–	9.6×10^{-5}, 600	1.06	21a
$La_{0.9}Sr_{0.1}Ga_{0.8}Mg_{0.2}O_{2.85}$	9.1×10^{-12}, 800	4.14	3.6×10^{-4}, 800	1.12	22

[a] Data obtained from second cycle (Figure 16).

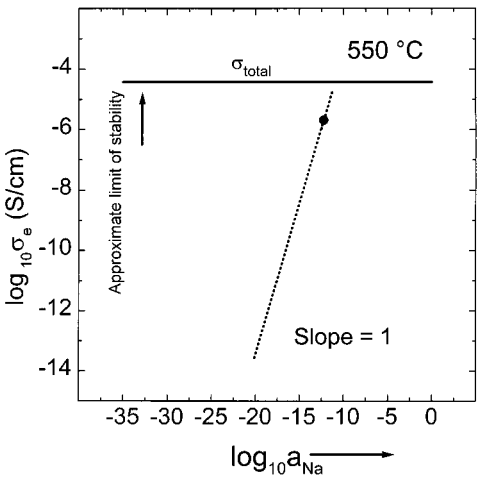

Figure 15. Dependencies of the conductivities at 550 °C of Na^+ ions and excess electrons in $NaCa_2Nb_3O_{10}$ on the sodium activity. The dotted line passing through the experimental data points is drawn with a slope of 1 according to eq 8. The hole conductivity as a function of sodium activity is not shown as it is assumed to be much smaller than of excess electronic conductivity.

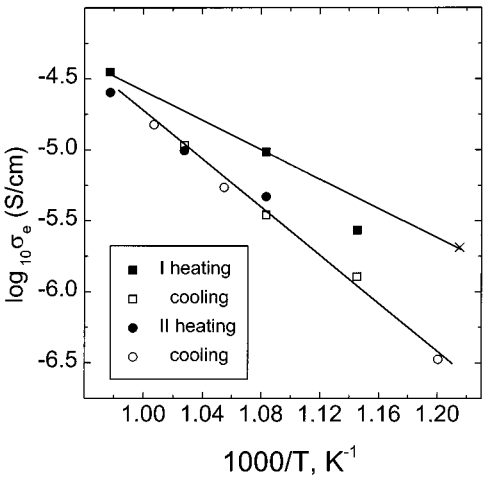

Figure 16. Arrhenius plots for the partial electronic conductivity of $NaCa_2Nb_3O_{10}$. One data point (×) obtained from Figure 8 is shown for comparison. The data obtained from the first cooling cycle and from the subsequent cycle follow the same line. The line connecting the data points is a guide to the eyes.

ments. The difference might be due to the possibility that the chemical potential of the sodium ions was not constant and that slight variations in the compositions of the two different samples occurred.

The variation of the electronic conductivity as a function of the activity of sodium is shown in Figure 15. We used a slope of 1 based on eq 8. In layered perovskites, at the investigated temperature of 550 °C, the estimated upper limit of sodium activity is about 10^{-10}, at which point the material shows predominantly ionic conductivity. The partial electronic conductivity as a function of temperature was measured by employing a second HW cell to which a fixed cell voltage of 1.3 V was applied. The data are shown in Figure 16. Those obtained from the first cycle of cooling and the second cycle of heating and cooling follow the same line. The data obtained during the second cycle are compared with literature values of well-known ionic conductors (Table 3). It can be seen that the presently observed activation energy for electron conduction, 1.68 eV, is comparable to the values for β-aluminas[13] and lower than those for anion conductors based on CeO_2,[15] ZrO_2,[11] and $LaGaO_3$.[21,22] The partial electronic conductivity is comparable to those of β-aluminas,[13] $Ce_{0.8}Gd_{0.2}O_{1.9}$, and $Ce_{0.8}Gd_{0.17}Pr_{0.03}O_{1.9}$ at about 600 °C.[15]

5. Conclusion

Hebb–Wagner polarization using $NaCoO_2$ as the reversible electrode and ac and dc measurements with electron-blocking Na-β-alumina electrodes show that the D–J-type layered perovskite $NaCa_2Nb_3O_{10}$ is a predominant ionic conductors for sodium ions. The transference number is close to unity. At a sodium activity of $\log a_{Na} = -10$, the total and electronic conductivities are of the same order of magnitude. The present detailed electrical investigation supports the assumption of ionic conductors presented on the basis of the ion-exchange reaction of layered perovskites. We also believe that the present work can be considered as being representative for lamellar oxides containing Nb in perovskite layers.

Acknowledgment. We thank Mrs. Marlies Schwitzke for the EDAX and SEM measurements. One of us (V.T.) thanks the Alexander von Humboldt Foundation for a Research Fellowship.

Note Added after ASAP Posting

This article was released ASAP on 2/21/2002 with a couple of errors in the equations. The correct version was posted on 2/25/2002.

CM011189W

(22) Kim, J. H.; Yoo, H. I. *Solid State Ionics* **2001**, *140*, 105.